Granular Matter (2019) 21:82
https://doi.org/10.1007/s10035-019-0931-5

ORIGINAL PAPER

Shear jamming and fragility in dense suspensions

Ryohei Seto[1] · Abhinendra Singh[2,3] · Bulbul Chakraborty[4] · Morton M. Denn[5] · Jeffrey F. Morris[5]

Received: 12 February 2019 / Published online: 2 August 2019
© Springer-Verlag GmbH Germany, part of Springer Nature 2019

Abstract
The phenomenon of shear-induced jamming is a factor in the complex rheological behavior of dense suspensions. Such shear-jammed states are fragile, i.e., they are not stable against applied stresses that are incompatible with the stress imposed to create them. This peculiar flow-history dependence of the stress response is due to flow-induced microstructures. To examine jammed states realized under constant shear stress, we perform dynamic simulations of non-Brownian particles with frictional contact forces and hydrodynamic lubrication forces. We find clear signatures that distinguish these fragile states from the more conventional isotropic jammed states.

Keywords Shear jamming · Suspension rheology · Granular physics

1 Introduction

Suspensions, in which solid particles are dispersed in a viscous liquid, are a class of complex fluids found frequently in nature, industry, and consumer applications [1, 2]. To predict flows of suspensions with arbitrary macroscopic boundary conditions, it is necessary to develop continuum models based on particle-scale physics; it is too expensive to simulate individual motions of particles and interstitial flows for macroscopic problems. Dilute suspensions, in which the solid volume fractions ϕ are less than about 5%, are well described with the Newtonian constitutive model with a modified viscosity [3, 4]. However, constitutive models for denser suspensions exhibiting more complex rheological properties are still not available [5, 6].

Suspensions are always liquid-like fluids below a certain volume fraction, i.e., there is no possibility to realize states exhibiting rigidity by any protocols. Conversely, it is possible to induce rigidity in suspensions above a certain solid volume fraction. Shear jamming is the phenomenon when shear strains yield such a rigidity [7–9]. *Fragile matter* as a constitutive class of complex fluids was introduced to describe emergence of rigidity in flowing suspensions [10, 11]. First, it is helpful to emphasize that there are only three possible states in non-Brownian suspensions of rigid particles regarding mechanical responses (see Fig. 1a):

(i) *liquid-like* state, that cannot statically bear any shear stress.
(ii) *solid-like* state, that can statically bear stresses in all directions.
(iii) *fragile* state, that can statically bear stresses only within a certain range of directions.

We assume sufficiently weak stresses (or infinitely rigid particles) in these classifications to exclude yielding. The unjammed states are liquid-like, and isotropically jammed states are solid-like. A number of processes may lead to these two states. On the other hand, fragile states are usually

This article is part of the Topical Collection: In Memoriam of Robert P. Behringer.

Electronic supplementary material The online version of this article (https://doi.org/10.1007/s10035-019-0931-5) contains supplementary material, which is available to authorized users.

✉ Ryohei Seto
setoryohei@me.com

[1] Department of Chemical Engineering, Kyoto University, Kyoto, Japan

[2] Benjamin Levich Institute, CUNY City College of New York, New York, USA

[3] Present Address: Pritzker School of Molecular Engineering and James Franck Institute, The University of Chicago, Chicago, USA

[4] Martin Fisher School of Physics, Brandeis University, Waltham, USA

[5] Benjamin Levich Institute and Department of Chemical Engineering, CUNY City College of New York, New York, USA

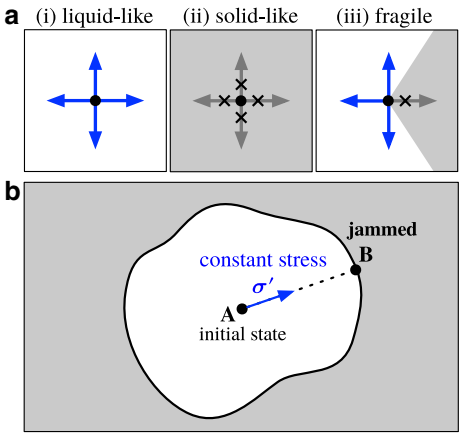

Fig. 1 **a** Three possible states of non-Brownian suspensions: (i) liquid-like, (ii) solid-like, and (iii) fragile, are defined according to distinct stress responses. Different directions indicate stresses of different compression/traction axes in this representation. **b** A schematic "phase space" of microstates (structures) of a suspension. A suspension is initially in a liquid-like state, represented by the point **A**. It flows under constant stress $\boldsymbol{\sigma}'$ and reaches a jammed state **B**. The gray domain is unreachable with constant stresses from **A**

associated with particular processes leading to fragile configurations. Let us consider an idealized system of rigid-particle suspensions. If we randomly pick a relaxed state (i.e., without flow-induced microstructure) below the isotropic jamming point, it should be liquid-like and flow under arbitrary shear stress $\boldsymbol{\sigma}'$. In the schematic configuration space shown in Fig. 1b, such an initial state is expressed as a point **A**. The trajectory (dashed line) indicates the shearing process due to $\boldsymbol{\sigma}'$, which passes through different particle configurations. The flow induces some microstructure to resist the applied stress, which slows down the flow, eventually bringing it to a stop; i.e., the system reaches a jammed state, **B**. This jammed state statically supports the stress $\boldsymbol{\sigma}'$, like an elastic or rigid solid; unlike deformed elastic materials, however, it is able to maintain the strain even after the stress is no longer applied. This jammed state is unstable against a change in the applied stress. Since we reached the jammed state **B** with the stress $\boldsymbol{\sigma}'$, we may reverse the deformation with the opposite stress $-\boldsymbol{\sigma}'$, at least to some extent. Thus, jammed states encountered in shearing processes under constant stresses seem to always be fragile. (In general, such jammed states may be able to support stress reoriented at a small angle of shear direction [12] or stress with the principal axes rotated in a small angle. However, the existence of one incompatible stress is enough to judge fragility; thus, we consider only shear stress reversal here.) If a different stress were to be applied to the initial state **A** from the beginning, the system would reach another jammed state. Such jammed states from **A** with different applied stresses form a surface, beyond which configurations are unreachable from **A**.

A shear-jammed state is one which is reached by shear but is then able to statically bear the shear stress (or 'load'). As this state is not statically stable for applied stresses incompatible with the jammed state, it is termed fragile in the terminology of Cates et al. [11], and we follow that terminology here; Fig. 1a (iii) illustrates the concept. Upon reversal of the shear stress from a fragile shear-jammed state, the suspension will flow, i.e., undergo some finite strain, before possibly reaching a jammed state in the new direction.

The occurrence of shear jamming under quasi-statically imposed strain was experimentally elucidated in frictional grains by Bi et al. [13], and its connection to Reynolds dilatancy was elaborated in Ren et al. [14]. Two types of shear-jammed states were identified at a given ϕ: states created at lower strains, which could not sustain shear reversal, and states at strains higher than a characteristic value, which could. In [13], the former were referred to as fragile and the latter as shear-jammed. Sarkar et al. [15–17] developed a theoretical framework to describe the transition between the two types of jammed states identified in [13]. Recent numerical work by Otsuki and Hayakawa [18] showed that this transition could be detected through imposition of oscillatory shear. It should be noted that those previous studies on shear jamming were performed with strain-controlled protocols, in which deformation is forced regardless of whether jammed or not. In contrast, we investigate shear jamming with a stress-controlled protocol; once a system is jammed, no further deformation occurs in the same direction. This stress-controlled approach seems, in this way, more natural to capture shear jamming than the previous works. (Very recently, Srivastava et al. [19] also investigated "shear-arrested states" using constant-stress discrete element simulations.) In this article, we examine fragility of shear jammed states by performing particle dynamics simulations with idealized conditions: inertialess, non-Brownian, and monolayer systems.

2 Simulation model

We consider suspended particles in a viscous liquid. The particles are sufficiently small for all inertial effects to be negligible, i.e., the Stokes number $St \equiv \rho a^2 \dot{\gamma}/\eta_0$ (with ρ and a being the density and radius of particles, respectively, $\dot{\gamma}$ being the shear rate, and η_0 being the viscosity of the suspending fluid) is vanishingly small. We also omit Brownian motions, which are relevant for smaller particles. Stokesian Dynamics (SD) is an efficient method to reproduce particle dynamics in this Stokes regime [20]. The viscosity divergence predicted by the original SD is a dynamic effect due to the singularity of hydrodynamic lubrication [21, 22]. Recently, the SD approach (with only hydrodynamic lubrication) was extended to be coupled with frictional contact

mechanics to reproduce discontinuous shear thickening [23]. In this work, we employ an algorithm to mimic stress-controlled rheology [24]. The viscosity divergence under a constant shear stress is just a consequence of a static force balance of the contact forces. In contrast to the original SD, the hydrodynamic contributions vanish at the viscosity divergence. Therefore, the results shown in this article would share some common features with dry granular systems in the quasi-static limit.

2.1 Stress-controlled quasi-static dynamics

Particles with negligible inertia suspended in a viscous liquid obey the force and torque balance equations of hydrodynamic and non-hydrodynamic interactions,

$$\boldsymbol{F}_{\mathrm{h}}(\boldsymbol{U}) + \boldsymbol{F}_{\mathrm{nh}} = \boldsymbol{0}, \tag{1}$$

where $\boldsymbol{U}$ represents the many-body linear and angular velocities of particles. In the zero-Reynolds number limit, the hydrodynamic interactions can be expressed as a linear resistance, $\boldsymbol{F}_{\mathrm{h}}(\boldsymbol{U}) = -\mathsf{R}_{\mathrm{FU}} \cdot \boldsymbol{U}$, where R_{FU} is the resistance matrix [20]. Thus, particles are moved with $\boldsymbol{U} = \mathsf{R}_{\mathrm{FU}}^{-1}\boldsymbol{F}_{\mathrm{nh}}$. For the case of very dense suspensions, R_{FU} can be approximately constructed with the pair-wise hydrodynamic lubrication [25, 26]. The lubrication coefficients are known to diverge when two spherical particles approach, but we regularize these interactions with a cutoff length [27].

With a background flow gradient of $\nabla\boldsymbol{u}$, the hydrodynamic interactions are modified to the sum of the linear resistances to the particle velocity deviations $\boldsymbol{U} - \boldsymbol{u}$ and to the rate-of-deformation tensor $\mathsf{D} \equiv (\nabla\boldsymbol{u} + \nabla\boldsymbol{u}^{\mathsf{T}})/2$,

$$\boldsymbol{F}_{\mathrm{h}}(\boldsymbol{U}) = -\mathsf{R}_{\mathrm{FU}} \cdot (\boldsymbol{U} - \boldsymbol{u}) + \mathsf{R}_{\mathrm{FD}} : \mathsf{D}, \tag{2}$$

where R_{FD} is also a resistance matrix [28]. Furthermore, the simulation cell with periodic boundary conditions needs to be deformed according to $\nabla\boldsymbol{u}$ (for more details see [29]).

As a consequence of the linearity of the governing equations, particle velocities $\boldsymbol{U}$ and the flow rate of a fixed flow type can be simultaneously determined under a given shear stress σ^{xy}. Here, we fix the flow type to simple shear flows, $\boldsymbol{u}(\boldsymbol{r}) = \dot{\gamma} y \boldsymbol{e}_x$, with shear rate $\dot{\gamma}$, which is the only degree of freedom to be determined in $\nabla\boldsymbol{u}$. The stress tensor can be expressed as the sum of the deformation contribution and contributions by non-hydrodynamic interactions,

$$\boldsymbol{\sigma} = \dot{\gamma}\hat{\boldsymbol{\sigma}}_{\mathrm{D}} + \boldsymbol{\sigma}_{\mathrm{nh}}, \tag{3}$$

in which the unknown shear rate $\dot{\gamma}$ is explicitly factored out from the first term. The rest is independent of $\dot{\gamma}$,

$$\hat{\boldsymbol{\sigma}}_{\mathrm{D}} = \frac{1}{V}\sum_i \left(\mathsf{R}_{\mathrm{SD}} : \hat{\mathsf{D}} + \mathsf{R}_{\mathrm{SU}} \cdot \hat{\boldsymbol{U}}_{\mathrm{D}}\right)^{(i)}, \tag{4}$$

with $\hat{\boldsymbol{U}}_{\mathrm{D}} = \mathsf{R}_{\mathrm{FU}}^{-1} \cdot \mathsf{R}_{\mathrm{FD}} : \hat{\mathsf{D}}$ and the normalized rate-of-deformation tensor $\hat{\mathsf{D}} \equiv \mathsf{D}/\dot{\gamma}$. The non-hydrodynamic contribution,

$$\boldsymbol{\sigma}_{\mathrm{nh}} = \frac{1}{V}\left\{\sum_{i>j}(\boldsymbol{r}_i - \boldsymbol{r}_j)\boldsymbol{F}_{\mathrm{nh}}^{(ij)} - \sum_i (\mathsf{R}_{\mathrm{SU}} \cdot \boldsymbol{U}_{\mathrm{nh}})^{(i)}\right\}, \tag{5}$$

is also independent of $\dot{\gamma}$, where $\boldsymbol{U}_{\mathrm{nh}} = \mathsf{R}_{\mathrm{FU}}^{-1} \cdot \boldsymbol{F}_{\mathrm{nh}}$. From the xy component of (3), we can determine $\dot{\gamma}$ for the given shear stress σ^{xy},

$$\dot{\gamma} = \frac{\sigma^{xy} - \sigma_{\mathrm{nh}}^{xy}}{\hat{\sigma}_{\mathrm{D}}^{xy}}. \tag{6}$$

Now, we can also determine the particle velocities with the obtained $\dot{\gamma}$: $\boldsymbol{U} = \dot{\gamma}\hat{\boldsymbol{U}}_{\mathrm{D}} + \boldsymbol{U}_{\mathrm{nh}}$.

2.2 Contact force model

In many stable suspensions used in practice, some repulsive forces act between non-contacting particles, preventing flocculation due to short-range van der Waals attractions. However, in this article, we focus on a simple model system in which the non-hydrodynamic interaction consists only of contact forces: $\boldsymbol{F}_{\mathrm{nh}} = \boldsymbol{F}_{\mathrm{c}}$.

To model $\boldsymbol{F}_{\mathrm{c}}$, we employ a soft-constraint approach. The first geometrical constraint is the volume excluding force of solid particles. Hard-sphere particles will have zero overlap. To mimic this, we introduce a harmonic penalty function $(k_{\mathrm{n}}/2)(a_i + a_j - r_{ij})^2$, which generates a force along the normal direction. Here, a_i and a_j are radii of particles i and j, and r_{ij} the distance between them.

When rough or bumpy solid surfaces are in contact, their sliding displacements are also restricted by friction or interlocking; here, we introduce another harmonic penalty function $(k_{\mathrm{t}}/2)\boldsymbol{\xi}^2$ of the relative sliding displacement $\boldsymbol{\xi}$, which is determined with translations and rotations of contacting particles [30]. This generates tangential forces acting at the contact point. Regarding the maximum tangential force, we employ a simple Coulomb friction law, where the upper bound is proportional to the normal force with a proportionality coefficient μ. In this work, we mainly study an infinite friction coefficient, implying that sliding displacements are constrained as long as the particles are pushed inward.

This soft-constraint approach is fundamentally different from hard-sphere algorithms, which impose strict geometrical constraints. To make the constraints stricter, we would need to set sufficiently large values for the penalty parameters k_{n} and k_{t}. The values which we selected keep the maximum overlap and tangential displacement less than 2% of the particle radius below the isotropic jamming point.

3 Results and discussion

We study monolayer bidisperse systems of 1000 spherical particles, with a size ratio of 1.4 and a volume ratio of approximately 1. To generate initial configurations, we used Brownian simulations to relax randomly placed particle configurations.

3.1 Shear reversal test

We start by confirming the concept of fragile matter with our simulation model for dense suspensions. To understand the roles of shear-induced structure, Gadala-Maria and Acrivos [31] performed shear reversal tests using a rate-controlled setup. Here, we simulate a stress-controlled shear reversal test.

We apply a constant stress $\sigma^{xy} = \sigma'$ to an equilibrated suspension of $\phi = 0.77$ (Fig. 2a). The strain evolution is relatively fast at the beginning of the simulation and eventually slows down (Fig. 2b). The slowly flowing state, say $|\dot{\gamma}| > 10^{-4}\dot{\gamma}_0$, lasts for a while. Fluctuation of $\dot{\gamma}$ in the flowing state indicates some restructuring of the stress-bearing contact network (Fig. 2c).

The system is shear-jammed when all particles are in static force balance $\boldsymbol{F}_{\mathrm{C}}^{(i)} = 0$ and a contact network to support all stress is formed such that $\sigma_{\mathrm{C}}^{xy} = \sigma^{xy}$. According to (1) and (6), these conditions lead to $\boldsymbol{U}^{(i)} = 0$ and $\dot{\gamma} = 0$. We consider states to be jammed with the following criteria: $\max|\boldsymbol{V}^{(i)}| < 10^{-3}a\dot{\gamma}_0$ and $|\dot{\gamma}| < 10^{-8}\dot{\gamma}_0$; the characteristic shear rate $\dot{\gamma}_0 \equiv \sigma'/\eta_0$ is used. Here, $\boldsymbol{V}^{(i)} \equiv \boldsymbol{U}^{(i)} - \boldsymbol{u}(\boldsymbol{r}^{(i)})$ are non-affine particle velocities. $\gamma_{\mathrm{J}}^{(1)}$ denotes the total strain to the shear-jammed (SJ) states from the relaxed initial configuration. Jamming occurs above the isostatic condition $Z > Z_{\mathrm{iso}}^{\mu=\infty} = 3$ [32], where Z is the average contact number with non-rattlers. Particles that have fewer than two contacts with non-rattlers are called rattlers, and thus we need some iteration to determine them. As seen in Fig. 2d, the isostatic condition does not immediately lead to the SJ state.

Now, we reverse the shear stress to $\sigma^{xy} = -\sigma'$, corresponding to a rotation of the principal stress axes by $\pi/2$. Since the previously formed contact network cannot support this new stress, the suspension unjams. The contact number drops to a value Z_{min}, being below the isostatic condition (Fig. 2d). Thus, the stress-reversal simulation confirms that the SJ state is *fragile*. We continue the simulation with $-\sigma'$. The particle dynamics is not reversible, and the state does not return to the initial configuration; rather, it reaches another SJ state after strain $\gamma_{\mathrm{J}}^{(2)}$.

After reaching the second jammed state, we stop applying the stress $\sigma^{xy} = 0$ to confirm the smallness of the elastic recovery strain (Fig. 2b). This small recovery is due to the finite values of the penalty parameters k_{n} and k_{t} in the soft-constraint contact model. In the ideal hard-sphere limit, the recovery strain will be zero. If stress is applied in the same direction again, the system will not flow because the contact network remains.

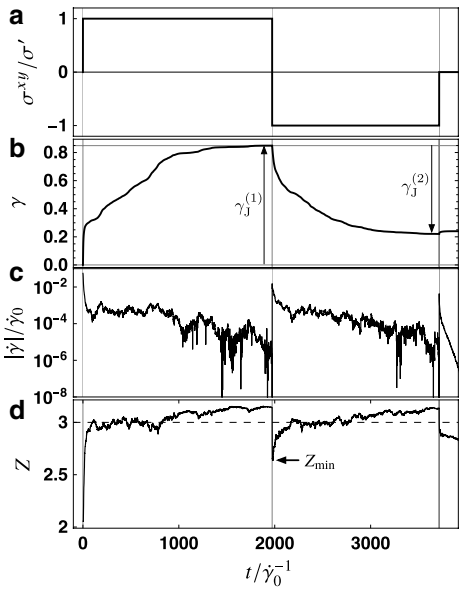

Fig. 2 Time series of **a** shear stress σ^{xy}, **b** shear strain γ, **c** absolute value $|\dot{\gamma}|$ of shear rate, and **d** contact number Z with non-rattlers in a stress-controlled shear reversal test at $\phi = 0.77$ with $\mu = \infty$. The shear stress is reversed after reaching the jammed state. After reaching the second jammed state, shearing is stopped. The unit of shear rate $\dot{\gamma}_0 \equiv \sigma'/\eta_0$ is used for the nondimensionalization

3.2 Features of shear-jammed states

The SJ state is realized due to formation of a stress-bearing contact network. The particle movements obey the force and torque balance equations (1), and rearrangements continue until static balances are globally achieved. The structural evolution to reach the global balance is not monotonic. As seen in the movie in Supplementary Material, a static force balance, which is roughly indicated by vanishing velocities (dark colors), is locally achieved in advance of other parts, but the local stress axes may change due to rearrangements of other parts. Thus, the local domains, which achieved a force balance once, need to be restructured again (cf. "micro-fragility" in [10]).

The strain γ_{J} to reach a SJ state reflects the difficulty in realizing the global force balance. Fig. 3a shows the area fraction dependence of $\gamma_{\mathrm{J}}^{(1)}$ from relaxed initial configurations to the first jammed states, and $\gamma_{\mathrm{J}}^{(2)}$ from the first to the second jammed states. Particle contacts to build a network are more accessible at higher area fractions, and shear jamming accordingly occurs at smaller strain. All

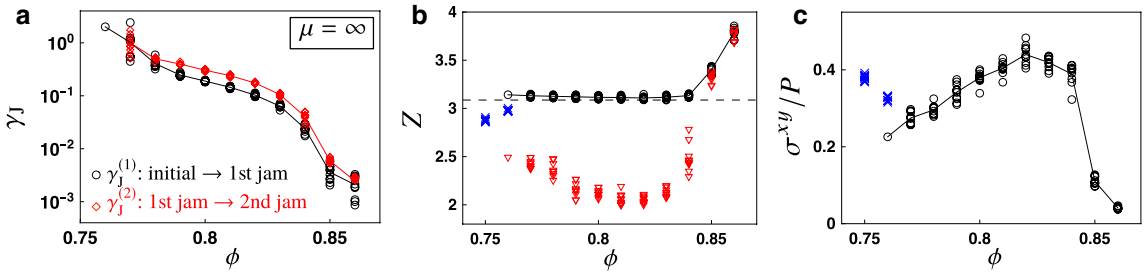

Fig. 3 **a** The larger is ϕ, the smaller is the average strain γ_J to reach a SJ state. $\gamma_J^{(1)}$ (circle) and $\gamma_J^{(2)}$ (red diamond) are strains to reach the first jammed states from the initial states and the second jammed states after stress reversals, respectively. Only jammed results of ten simulations are plotted. **b** Mean contact number Z with non-rattlers of SJ states (circle) are almost constant for $\phi \leq 0.84$. The lowest value of the SJ states is $Z \approx 3.07$ (dashed line). These SJ states can be confirmed as fragile with the minimum values Z_{min} after the shear reversals (red downtriangle) (see Fig. 2d), which are below the isostatic condition $Z_{iso} = 3$ for $\phi \leq 0.84$. Z of unjammed states (blue ×'s) are below but close to the plateau value near the boundary. **c** The sharp decrease of the stress anisotropy σ^{xy}/P of jammed states (circle) above $\phi = 0.84$ indicates the transition from shear jamming to isotropic jamming [15–17] (color figure online)

simulations for $\phi \geq 0.77$ indeed end up in jammed states, but require larger γ_J for lower ϕ. Only one of ten simulations at $\phi = 0.76$, and none at $\phi = 0.75$, were jammed within the given maximum strain $\gamma_{max} = 5$. Thus, the threshold area fraction ϕ_{SJ} to realize SJ states is expected to be in the range $0.75 < \phi_{SJ} < 0.76$, although based on the results available we cannot rule out the possibility of eventual shear jamming at $\phi = 0.75$ or even lower.

Though the isostatic condition $Z = Z_{iso}$ (= 3 for $\mu = \infty$) alone does not determine whether or not shear jamming occurs, shear jamming was realized at slightly larger $Z \approx 3.1$ in all of our simulations for $\phi \leq 0.84$ (Fig. 3b). If we were to run more simulations with larger γ_{max}, the minimum line of Z might approach the isostatic condition. (The SJ state at the lowest possible ϕ may be close to random loose packing [33, 34], but is anisotropic owing to the shearing by which it is accessed.) We can confirm fragility with the minimum value (red downtriangle) of Z after the stress reversal. If Z goes below Z_{iso}, the system must experience liquid-like states no matter how short their duration.

3.3 Isotropic jamming

Strains to achieve jammed states become progressively lower at higher area fractions (Fig. 3a). The strains $\gamma_J^{(1)}$ are less than 0.01 at $\phi \geq 0.85$, and higher penalty parameters for the contact model, k_n and k_t, can make them even lower (data are not shown). The vanishing value of $\gamma_J^{(2)}$ suggests that the state does not flow in any direction, i.e., the jammed state is solid-like. As seen in Fig. 3c, the stresses of these states indeed become more isotropic (The ratio σ^{xy}/P is one way to represent the stress anisotropy, where P is the particle pressure [35]). We can also see the sudden increase in Z above $\phi = 0.85$ (Fig. 3b). These observations suggest that the solid-like jammed states are obviously distinguishable from the SJ state, but similar to the conventional isotropically jammed state despite the presence of friction. The transition point ϕ_{IJ} seems to be in the range $0.84 < \phi_{IJ} < 0.85$, which agrees with the known value (about 0.84) for frictionless 2D systems [36].

3.4 Stress-bearing structure

Figure 4a shows stress transmission patterns bearing σ' in the first jammed states (upper) and $-\sigma'$ in the second jammed states (lower), respectively. The superposition of stressed particles in the first and second jammed states (Fig. 4b) displays how stress bearing structures are different at $\phi = 0.77$ and 0.83 but more similar at $\phi = 0.85$. The anisotropy, which may be noticed at $\phi = 0.77$ and 0.83 in Fig. 4a, is confirmed with the angular distributions for the orientation of contacting stressed particles (Fig. 4c). In this way, fragile SJ states require some compatible anisotropic structures; thus they are renewed to adapt to the opposite direction of the applied stress.

3.5 Friction

So far we have focused on the theoretical limit of frictional systems with $\mu = \infty$. We briefly discuss the μ dependence of our results. As seen in Fig. 5a, the shear jamming was achieved only when $\mu \geq 0.5$ at $\phi = 0.8$, which indicates that ϕ_{SJ} shifts to higher values with a weaker friction μ as we already saw [28, 9]. The strain γ_J to reach SJ states increases with smaller μ. More contacts Z are required to realize jamming (Fig. 5b). We also notice that the contact number Z of unjammed states increases with μ; particles tend to contact in frustrated flows due to friction.

Even when friction is completely absent ($\mu = 0$), we obtained a similar shear-jamming phenomenology; the systems are shear-jammed after some flow (Fig. 6a), and the contact numbers Z of jammed states drop to below the

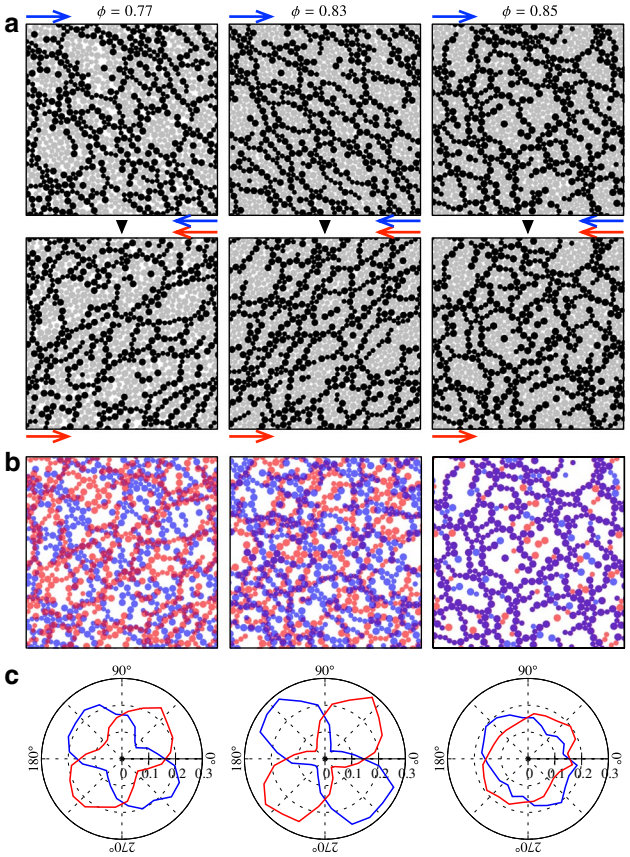

Fig. 4 **a** Stress transmission patterns of the first jammed states under $\sigma^{xy} = \sigma'$ (upper) and the second jammed states under $\sigma^{xy} = -\sigma'$ (lower) are shown. Stressed particles, $P^{(i)} > \langle P \rangle$, are in black, where $P^{(i)} \equiv -\mathrm{Tr}\,\boldsymbol{\sigma}^{(i)}/2$ is particle pressure of the i-th particle. **b** Stressed particles in the first (blue) and second (red) jammed states are imposed. Overlapping particles appear in purple. **c** The polar plots show the probabilities of the orientation between two contacting stressed particles in the first (blue) and the second (red) jammed states. The distributions are obtained from 10 simulations. The polar plots grow more anisotropic from $\phi = 0.77$ to 0.83, but become more isotropic at $\phi = 0.85$ (color figure online)

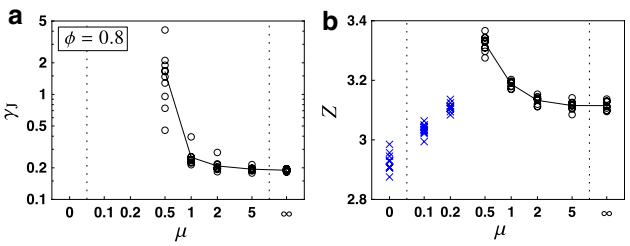

Fig. 5 **a** Friction coefficient μ dependence of the shear jamming strain γ_J (circle) at $\phi = 0.8$. Suspensions with lower frictions ($\mu = 0.2$ and below) did not reach jamming at this area fraction. **b** The contact number Z (blue ×'s) of unjammed states increases with the friction coefficient μ. However, lower Z (circle) is required to realize jammed states with higher μ (color figure online)

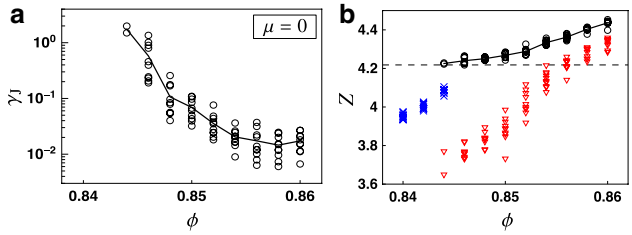

Fig. 6 **a** Strains γ_J to reach jammed states for frictionless suspensions ($\mu = 0$). **b** The average contact numbers Z (circle) monotonically increase as the volume fraction ϕ. SJ states may be indicated by the minimum values after the shear reversal (red downtriangle) which are below the isostatic condition $Z_{\mathrm{iso}} = 4$. However, the observed range of area fractions is rather narrow. Z of unjammed states are time-averaged values (blue ×'s) (color figure online)

isostatic condition ($Z_{\mathrm{iso}}^{\mu=0} = 2d$) after the stress reversal (Fig. 6b). However, this occurs in a narrow range just below the isotropic jamming. Our particles seem too soft to see a clear transition from the shear jamming to the isotropic jamming. As discussed elsewhere [37], the shear jamming observed in frictionless particles can be just due to a finite size effect. Thus, our current simulation cannot confirm the existence of shear jamming without friction.

4 Conclusions

We confirmed that dense suspensions with frictional interactions between particles can behave as fragile matter. In a flowing dense suspension under stress, a contact network is formed. The suspension becomes jammed when the shear-induced contact network statically supports the entire stress. However, this jammed state is not stable; a change of stress axes makes it flow. This fragile instability is the most important feature of shear jamming to be distinguished from the solid-like isotropic jamming. Furthermore, we found various signatures to distinguish the two different states in the average contact number Z, the drop of Z after the stress reversal, and the stress anisotropy σ^{xy}/P. It is also worth noting that SJ states near the lower bound are truly "fragile." We need to set a sufficiently short time step to capture such SJ states in simulations with the soft-constraint contact model.

In this article, we did not investigate the dependence on the strength $|\sigma^{xy}|$ of the shear stress. Ideal inertialess hard-sphere suspensions do not possess any internal force scale; thus, the states must be independent of the stress scale. Therefore, in the phase diagram with stress and area fraction, shear jamming lies in the vertical boundaries: $\phi_{\mathrm{SJ}} < \phi < \phi_{\mathrm{IJ}}$. If some interparticle repulsive forces or Brownian forces act on particles, they tend to hinder the formation of a contact network. This competition introduces a stress dependence.

Deformability of particles also causes a similar stress dependence; contact deformation can enhance tangential constraints restricting sliding and rolling degrees of freedom [11]. It is worth noting the distinction between shear thickening and Reynolds dilatancy here [38]. Shear thickening does require such an internal force scale besides tangential constraints; this makes the rheology of suspensions rate dependent [23]. Shear jamming is relevant to shear thickening but is a more basic phenomenon; it can occur just due to shear strain without the internal force scale, as demonstrated in this article. Since the volume of a suspension is constrained, shear jamming of dense suspensions can be considered as a confined Reynolds dilatancy [39].

Acknowledgements The authors would like to thank M. Otsuki, H. Hayakawa, and R. Mari for fruitful discussions. This study was supported by the Japan Society for the Promotion of Science (JSPS) KAKENHI Grants Nos. 17H01083 and 17K05618. BC was supported by NSF-CBET-1605428, while JFM was supported by NSF-CBET-1605283. The research was also supported in part by the National Science Foundation under Grant No. NSF PHY-1748958. RS thanks R. Yamamoto for his full support.

Compliance with ethical standards

Conflict of interest The authors declare that they have no conflict of interest.

References

1. Denn, M.M., Morris, J.F., Bonn, D.: Shear thickening in concentrated suspensions of smooth spheres in newtonian suspending fluids. Soft Matter **14**, 170–184 (2018)
2. Guazzelli, É., Pouliquen, O.: Rheology of dense granular suspensions. J. Fluid Mech. **852**, P1 (2018)
3. Einstein, A.: Eine neue bestimmung der moleküldimensionen. Ann. Phys. **19**, 289–305 (1906)
4. Einstein, A.: Berichtigung zu meiner arbeit: 'eine neue bestimmung der moleküldimensionen'. Ann. Physik **34**, 591–592 (1911)
5. Denn, M.M., Morris, J.F.: Rheology of non-brownian suspensions. Annu. Rev. Chem. Biomol. Eng. **5**(1), 203–228 (2014)
6. Goddard, J.D.: A dissipative anisotropic fluid model for non-colloidal particle dispersions. J. Fluid Mech. **568**, 1–17 (2006)
7. Bertrand, E., Bibette, J., Schmitt, V.: From shear thickening to shear-induced jamming. Phys. Rev. E **66**(6), 060401 (2002)
8. Peters, I.R., Majumdar, S., Jaeger, H.M.: Direct observation of dynamic shear jamming in dense suspensions. Nature **532**, 214 (2016)
9. Singh, A., Mari, R., Denn, M.M., Morris, J.F.: A constitutive model for simple shear of dense frictional suspensions. J. Rheol. **62**(2), 457–468 (2018)
10. Cates, M.E.: Stress transmission in jammed and granular matter, p. 369. IOP Publishing, Bristol (2000)
11. Cates, M.E., Wittmer, J.P., Bouchaud, J.P., Claudin, P.: Jamming, force chains, and fragile matter. Phys. Rev. Lett. **81**, 1841–1844 (1998)
12. Ness, C., Mari, R., Cates, M.E.: Shaken and stirred: random organization reduces viscosity and dissipation in granular suspensions. Sci. Adv. **4**(3), eaar3296 (2018)
13. Bi, D., Zhang, J., Chakraborty, B., Behringer, R.P.: Jamming by shear. Nature **480**, 355–358 (2011)
14. Ren, J., Dijksman, J.A., Behringer, R.P.: Reynolds pressure and relaxation in a sheared granular system. Phys. Rev. Lett. **110**, 018302 (2013)
15. Sarkar, S., Bi, D., Zhang, J., Behringer, R., Chakraborty, B.: Origin of rigidity in dry granular solids. Phys. Rev. Lett. **111**(6), 068301 (2013)
16. Sarkar, S., Bi, D., Zhang, J., Ren, J., Behringer, R.P., Chakraborty, B.: Shear-induced rigidity of frictional particles: analysis of emergent order in stress space. Phys. Rev. E **93**, 042901 (2016)
17. Sarkar, S., Chakraborty, B.: Shear-induced rigidity in athermal materials: a unified statistical framework. Phys. Rev. E **91**(4), 042201 (2015)
18. Otsuki, M., Hayakawa, H.: Shear jamming, discontinuous shear thickening, and fragile state in dry granular materials under oscillatory shear. arXiv:1810.03846 [cond-mat.soft] (2018)
19. Srivastava, I., Silbert, L.E., Grest, G.S., Lechman, J.B.: Flow-arrest transitions in frictional granular matter. Phys. Rev. Lett. **122**, 048003 (2019)
20. Brady, J.F., Bossis, G.: Stokesian dynamics. Annu. Rev. Fluid Mech. **20**(1), 111–157 (1988)
21. Melrose, J.R., Ball, R.C.: The pathological behaviour of sheared hard spheres with hydrodynamic interactions. Europhys. Lett. **32**, 535–540 (1995)
22. Morris, J.F.: Lubricated-to-frictional shear thickening scenario in dense suspensions. Phys. Rev. Fluids **3**, 110508 (2018)
23. Seto, R., Mari, R., Morris, J.F., Denn, M.M.: Discontinuous shear thickening of frictional hard-sphere suspensions. Phys. Rev. Lett. **111**, 218301 (2013)
24. Mari, R., Seto, R., Morris, J.F., Denn, M.M.: Nonmonotonic flow curves of shear thickening suspensions. Phys. Rev. E **91**, 052302 (2015)
25. Ball, R.C., Melrose, J.R.: A simulation technique for many spheres in quasi-static motion under frame-invariant pair drag and Brownian forces. Physica A **247**(1), 444–472 (1997)
26. Jeffrey, D.J., Onishi, Y.: Calculation of the resistance and mobility functions for two unequal rigid spheres in low-Reynolds-number flow. J. Fluid Mech. **139**, 261–290 (1984)
27. Wilson, H.J., Davis, R.H.: Shear stress of a monolayer of rough spheres. J. Fluid Mech. **452**, 425–441 (2002)
28. Mari, R., Seto, R., Morris, J.F., Denn, M.M.: Shear thickening, frictionless and frictional rheologies in non-Brownian suspensions. J. Rheol. **58**(6), 1693–1724 (2014)
29. Seto, R., Giusteri, G.G., Martiniello, A.: Microstructure and thickening of dense suspensions under extensional and shear flows. J. Fluid Mech. **825**, R3 (2017)
30. Luding, S.: Cohesive, frictional powders: contact models for tension. Granul. Matter **10**, 235–246 (2008)
31. Gadala-Maria, F., Acrivos, A.: Shear-induced structure in a concentrated suspension of solid spheres. J. Rheol. **24**(6), 799–814 (1980)
32. Henkes, S., van Hecke, M., van Saarloos, W.: Critical jamming of frictional grains in the generalized isostaticity picture. Europhys. Lett. **90**(1), 14003 (2010)
33. Ciamarra, M.P., Coniglio, A.: Random very loose packings. Phys. Rev. Lett. **101**, 128001 (2008)
34. Onoda, G.Y., Liniger, E.G.: Random loose packings of uniform spheres and the dilatancy onset. Phys. Rev. Lett. **64**, 2727–2730 (1990)
35. Giusteri, G.G., Seto, R.: A theoretical framework for steady-state rheometry in generic flow conditions. J. Rheol. **62**(3), 713–723 (2018)

36. Behringer, R.P., Chakraborty, B.: The physics of jamming for granular materials: a review. Rep. Prog. Phys. **82**(1), 012601 (2019)
37. Baity-Jesi, M., Goodrich, C.P., Liu, A.J., Nagel, S.R., Sethna, J.P.: Emergent SO(3) symmetry of the frictionless shear jamming transition. J. Stat. Phys. **167**(3), 735–748 (2017)
38. Barnes, H.A.: Shear-thickening ("Dilatancy") in suspensions of nonaggregating solid particles dispersed in Newtonian liquids. J. Rheol. **33**(2), 329–366 (1989)
39. Reynolds, O.: On the dilatancy of media composed of rigid particles in contact, with experimental illustrations. Philos. Mag. **20**(5), 469–481 (1885)

Publisher's Note Springer Nature remains neutral with regard to jurisdictional claims in published maps and institutional affiliations.